Progress In Electromagnetics Research, Vol. 122, 155–173, 2012

A NOVEL NON-INTERPOLATION POLAR FORMAT ALGORITHM USING NON-LINEAL FLIGHT TRAJECTORIES AND AUTO-ADAPTIVE PRF TECHNIQUE

Y. Wang*, J. W. Li, J. Chen, H. P. Xu, and B. Sun

School of Electronic and Information Engineering, Beihang University, Beijing, China

Abstract—The classical interpolation-based Polar Format Algorithm (PFA) for spotlight synthetic aperture radar (SAR) results in numerous computation load, which, reduces processing speed and increase system complexity. To decrease computation load, this paper proposes a novel non-interpolation PFA algorithm for sensor flying along non-lineal flight trajectories, which are specially designed curves in conical surface. Then an innovative auto-adaptive Pulse Repetition Frequency (PRF) technique is put forward to uniformly sample signal in azimuth direction. The computation load of the new PFA is merely left to azimuth chirp z-transforms (CZTs) and range fast Fourier transforms (FFTs) after dechirp processing and residual video phase (RVP) compensation. Two flight modes (ellipse trajectory mode and hyperbola trajectory mode) are analyzed. A lineal approximation method is proposed to simplify non-lineal sensor trajectory analysis. Computer simulation results for multiple point targets validate the presented approach. Comparison of computation load between this PFA and traditional PFA is represented in Appendix B.

1. INTRODUCTION

Synthetic Aperture Radar (SAR) is a remote sensing instrument offering high azimuth and range resolution radar images. In spotlight mode SAR, the sensor steers its antenna beam to continuously illuminate the terrain patch, providing longer illumination time to acquire higher azimuth resolution. SAR is proved to be more and more important either in commercial or military applications, e.g.,

Received 28 September 2011, Accepted 26 October 2011, Scheduled 17 November 2011
* Corresponding author: Yan Wang (yanwangbuaa@gmail.com).

target recognition [1], earth terrain classification [2], ocean monitory [3] and moving target detection [4–6]. Various algorithms have been applied in spotlight SAR image formation, including Back Projection Algorithm (BPA), the Frequency Scaling Algorithm (FSA), the Chirp Scaling Algorithm (CSA), the Range Migration Algorithm (RMA) and the Polar Format Algorithm (PFA) [7–13]. PFA is a widely used algorithm specially designed for spotlight SAR. The traditional PFA employs interpolation technique to convert data from polar format to rectangular format, leading to numerous computational load. In case of a 8-point interpolation, 8 complex multiplications and 7 complex additions are required for each datum sampled. This point-by-point computation method results in heavy pressure on signal processor, which limits processing speed and increases system complexity.

To decrease computation load, this paper presents a novel PFA using specially designed non-linear flight trajectory of the sensor, which enables a fast image formation algorithm without interpolation. In this algorithm, the sensor is designed to move in conical surface with cone vertex at the illuminated center point. In this way, data sampled after dechirp processing are uniformly distributed along azimuth direction in wavenumber domain without interpolation. Considering the characteristics of the flight trajectory, two cases are specially discussed. When the sensor moves in plane perpendicular to the ground, the flight path is shaped to part of an ellipse. When the sensor move in a fixed altitude, the flight path is shaped to one piece of a hyperbola intersected by plane parallel with ground and a conical surface. Taking advantage of such flight trajectories, interpolation-based resample processing can be avoided.

Due to the non-uniform interval resulting from the curved trajectory of sensors movement, an auto-adaptive PRF technique is employed to acquire data uniformly distributed in azimuth direction. Firstly, azimuth sampling positions are designed to be uniformly arranged. Then time intervals of every two adjacent sample points with a constant velocity of sensor are computed. Based on time interval variation discipline, special functions could be designed for time controlling. To achieve higher precise in computation, CZT is used to replace sinc-interpolation to uniformly display azimuth data. Then range FFTs will finish the process.

The total computation load of the process merely includes range FFTs and azimuth CZTs, which saves as half of computation load as what is in traditional PFA. The advantage of less computation load with the novel PFA indicates its potential suitability in real-time imaging applications, e.g., helicopter-borne SAR and lows speed UAV surveillance system. Since there is no special requirement for squint

angle, the sensor can image the interested area at high squint angle. Moreover, as interpolation operation can be saved, less accumulated error could be added in intermediate processing steps. This advantage can contribute to a higher range and azimuth resolution.

This paper is organized as follows. The disadvantages of the traditional PFA are briefly analyzed in Section 2. Trajectory derivation of two flight modes are presented in Section 3. A CZT-based azimuth processing method using auto-adaptive PRF technique is proposed in Section 4. Multiple point targets simulation results are presented and analyzed in Section 5, including scene limit analysis and potential platforms. The paper is summarized in Section 6 and suggestions for possible future work are put forward.

2. TRADITIONAL PFA ALGORITHM FOR SPOTLIGHT SAR

Consider the Spotlight mode SAR geometry of Figure 1. The origin of Descartes coordinate is set at the center reference point (CRP) of image scene. The XOY ground plane is the target focus plane. R_{ref} is the distance from the antenna phase center (APC) to the centre reference point. R is the distance between APC and a certain scatter. α denotes the angle between the negative Y axis and the direction from origin to the projection of APC on XOY plane. β is the slope angel between the ground plane (XOY) and the slant range plane. Black triangles indicate ground scatters within the illuminated area.

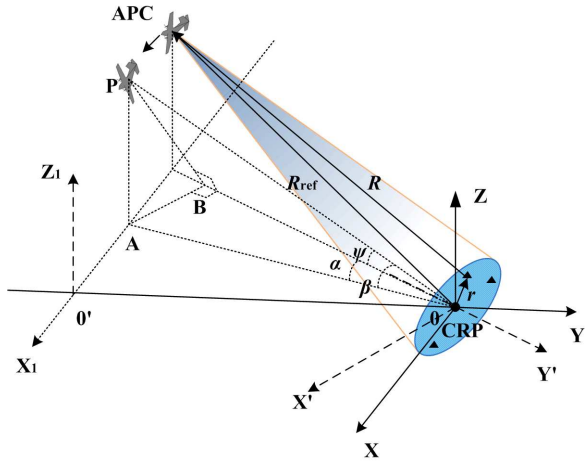

Figure 1. Spotlight mode SAR geometry.

Assume that the echoed dechirp pulse is given by

$$\begin{aligned} s_{if}(\tau,t) &= s_r(\tau,t)\cdot s^*_{ref}(\tau,t) \\ &= \exp\left\{-j\frac{4\pi}{c}\left(f_c+\gamma\left(\tau-\frac{2R_{ref}(t)}{c}\right)\right)R_\Delta(t)\right\} \\ &\quad \exp\left\{j\frac{4\pi\gamma}{c^2}R^2_\Delta(t)\right\} \\ R_\Delta(t) &= R(t)-R_{ref}(t) \end{aligned} \tag{1}$$

where τ is the fast (range) time and t is the slow (azimuth) time. f_c and γ are the carrier frequency and chirp rate, respectively. $R(t)$ indicates distance from APC to a certain scatter.

The second term is called residual video phase (RVP), which can be compensated by frequency-domain matched filter [14].

Overlooking effects caused by curved wavefront, phase in wavenumber domain can be expressed as follow

$$\begin{aligned} \phi &= Ka\cos\beta(\cos\gamma\sin\alpha+\sin\gamma\cos\alpha)=\cos\beta\,(K_x x+K_y y) \\ K &= \frac{4\pi}{c}\left(f_c+\gamma\left(\tau-\frac{2R_{ref}(t)}{c}\right)\right) \end{aligned} \tag{2}$$

where α, β, γ are shown in Figure 1. K_x and K_y indicate projection of K on X and Y axes, respectively.

Based on traditional PFA algorithm, a 2-D sinc-interpolation is always employed to implement resampling in wavenumber domain to convert data from polar format to rectangular format (shown in Figure 2). To release computation load, such a 2-D interpolation is usually replaced by two cascade 1-D interpolations. Figure 3 shows the steps of traditional PFA.

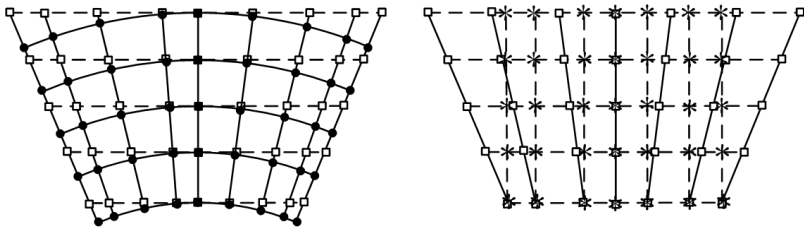

(a) Range interpolation (b) Azimuth interpolation

Figure 2. Interpolation from polar format to rectangular format.

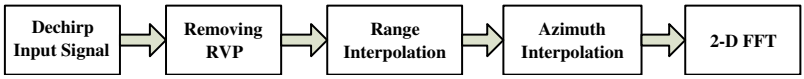

Figure 3. Tradition PFA algorithm based on interpolation method.

However, 2-D and 1-D sinc-interpolation will both lead to heavy computation load. In rotated Line-Of-Sight Polar Interpolation (LOSPI) coordinate, azimuth positions are non-uniformly distributed, and CZT cannot be directly used. For this matter, traditional PFA can hardly be used in any real-time system, which, as a result, may limit its applications. To avoid interpolation process, this paper presents a novel method by using specially designed flight trajectory as introduced in Section 3. To uniformly arrange data along azimuth direction, an auto-adaptive PRF technique is put forward as shown in Section 4.

3. FAST PFA ALGORITHM WITH NONLINEAR MOTION

Equation (3) shows that the projection of K is an azimuth-changing parameter in XOY plane though it remains a constant in 3-D space. Range interpolation is necessary because data need to be converted from polar format to rectangular format. Polar angle could be used to project K to X and Y axes in XOY plane. However, such necessity is based on restrictions that carrier frequency f_c, chirp rate γ are constants and sensor flies along a straight line. If things no longer follow such restrictions, some innovative flight modes can be specially designed, which can avoid range interpolation by saving half of the entire computation amount.

To design flight mode free of range interpolation, projection of K on Y direction should be a constant along azimuth direction for each range gate (shown as Figure 2(a)). Work presented here focuses on method of designing flight trajectory of sensor to achieve fast PFA algorithm.

Sampling echo wave after dechirp processing,

$$S_{if}(k,n) = \exp\left\{-j\left[K(k,n)(R(n)-R_{ref}(n)) - \frac{4\pi\gamma}{c^2}(R(n)-R_{ref}(n))^2\right]\right\} \quad (3)$$

where k and n are range and azimuth sampling array serial numbers respectively.

$$K(k,n) = \left[\frac{4\pi f_c}{c} + \frac{4\pi\gamma}{c}\left(\tau(k) - \frac{2R_{ref}(n)}{c}\right)\right] \quad (4)$$

Projection of $K\ (k,n)$ on Y direction is

$$K_y(k,n) = K(k,n)\cos\beta(n)\cos\alpha(n) \tag{5}$$

Definition of R, R_{ref}, α, β are shown in Figure 1. Equation (5) indicates that $\cos\beta(n)\cos\alpha(n)$ should remain a constant along the entire synthetic aperture time.

In geometry shown in Figure 1, the origin of Descartes coordinate is located at the CRP of illuminated area. Parameters have the following relationship

$$\cos\beta(n)\cos\alpha(n) = \frac{|OA|}{|OP|}\cdot\frac{|OB|}{|OA|} = \frac{|OB|}{|OP|} = \cos\psi(n) \tag{6}$$

This is to say, in 3-D geometry, sensor needs to move in a conical surface to make $\cos\beta(n)\cos\alpha(n)$ a constant. The vertex of the cone is the CRP and the symmetry axis overlaps with Y axis. The cone angle ψ can be expressed as

$$\psi = \arccos\left(\cos\beta(n)\cos\alpha(n)\right) \tag{7}$$

3.1. Ellipse Trajectory Mode

In this configuration, sensor moves in plane perpendicular with Y axis. The altitude of sensor will be changing within the entire synthetic aperture time. We assume that the Y coordinate of sensor at central

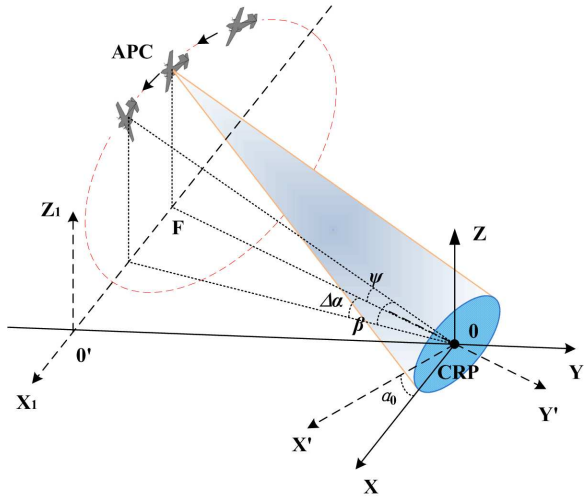

Figure 4. Sensor flights within plane parallel with XOZ plane.

synthetic aperture time is not zero. The flight trajectory intersected by plane $y = y_0$ and conical surface forms an ellipse as analyzed in Appendix A. The symmetry axis of the cone is the projection of LOS at central synthetic aperture time on XOY plane as shown in Figure 4.

Based on conic theory, point F should be the focal point of ellipse. Y' is the symmetry axis of cone. The ellipse can be depicted using α_0 and ψ. Based on Appendix A, the ellipse can be expressed as

$$\frac{z^2}{C + \frac{B^2}{A}} + \frac{\left(x - \frac{By_0}{A}\right)^2}{\frac{C}{A} + \frac{B^2}{A^2}} = 1 \tag{8}$$

where

$$\begin{aligned} A &= \cos^2\alpha_0 - \sin^2\alpha_0 \tan^2\psi \\ B &= y_0 \sin\alpha_0 \cos\alpha_0 \left(\tan^2\psi + 1\right) \\ C &= y_0^2 \left(\cos^2\alpha_0 \tan^2\psi - \sin^2\alpha_0\right) \end{aligned} \tag{9}$$

In order to get azimuth position of sensor, we have

$$\cos\beta(n) = \frac{\cos(\psi)}{\cos\left(\Delta\alpha(n) + \alpha_0\right)} \tag{10}$$

where α_0 is the value of α at zero synthetic aperture time; $\Delta\alpha(n) = \alpha - \alpha_0$. Then azimuth position $x(n)$ can be expressed as follows

$$\begin{aligned} x(n) &= R\cos\beta(n)\sin(\Delta\alpha(n) + \alpha_0) \\ &= R\cos\psi \frac{\cos\alpha_0 \tan(\Delta\alpha(n)) + \sin\alpha_0}{\cos\alpha_0 - \sin\alpha_0 \tan(\Delta\alpha(n))} \\ n &= -\frac{N_a}{2}, \ldots, -\frac{N_a}{2} \end{aligned} \tag{11}$$

where N_a denotes the total azimuth sampling number.

Especially when α_0 has a zero value, ellipse trajectory will be shaped to a circle, in which sensor illuminates the area with a zero squint angle in centre synthetic aperture time.

3.2. Hyperbola Trajectory Mode

In this mode, sensor moves in a fixed altitude, and the flight trajectory is shaped by intersection line of cone with vertex at CRP and plane parallel with XOY plane. According to conic theory, such a line is one piece of hyperbola. At central synthetic aperture time, LOS is orthogonal to flight direction. Figure 5 depicts this geometry.

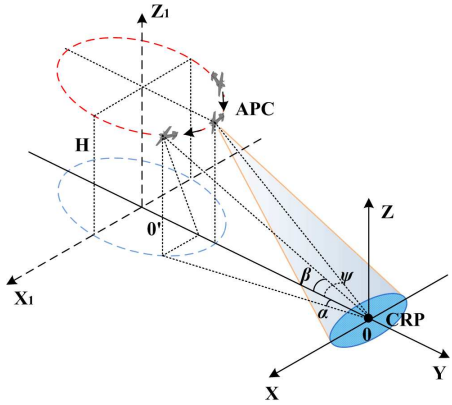

Figure 5. Sensor flights within plane parallel with XOY plane.

In geometry depicted in Figure 5, points on hyperbola satisfy the following equation:

$$\begin{cases} y^2 \tan^2 \psi = x^2 + z^2 \\ z = H \end{cases} \tag{12}$$

where $(x,\ y,\ z)$ is coordinate of an arbitrary point; H is sensor's altitude. Then intersect line can be achieved

$$\frac{y^2}{\frac{H^2}{\tan^2 \psi}} - \frac{x^2}{H^2} = 1 \tag{13}$$

Similar to ellipse trajectory mode

$$\beta(n) = \arccos\left(\frac{\cos\psi}{\cos(\Delta\alpha(n))}\right) \tag{14}$$

And the azimuth coordinate $x(n)$ can be expressed as

$$\begin{aligned} x(n) &= R\cos\beta(n)\sin(\Delta\alpha(n)) = H\cot\beta(n)\sin(\Delta\alpha(n)) \\ n &= -\frac{N_a}{2}, \ldots, -\frac{N_a}{2} \end{aligned} \tag{15}$$

where N_a is the number of total azimuth sampling points.

Azimuth coordinate $x(n)$ can be achieved as

$$\begin{aligned} x(n) &= x'(n)\cos\alpha_0 - y'(n)\sin\alpha_0 \\ &= H\cot\beta(n)\sin(\Delta\alpha(n))\cos\alpha_0 - \frac{H}{\sin\beta(n)}\cos\psi\sin\alpha_0 \end{aligned} \tag{16}$$

Then the sensor's trajectory and azimuth coordinate can be computed in both ellipse trajectory mode and hyperbola trajectory mode. The echo signal free of range interpolation is achieved as

$$S_{if}(k,n) = \exp\left\{-j\frac{4\pi}{c}\left(f_c + k\frac{B}{2N_r}\right)\left(x\tan\left(n\frac{\Delta\alpha_{\max}}{N_a}\right) + y\right)\right\} \quad (17)$$
$$k = -\frac{N_r}{2},\ldots,-\frac{N_r}{2};\quad n = -\frac{N_a}{2},\ldots,-\frac{N_a}{2}$$

where N_r is the number of entire range sample points, B is the bandwidth of dechirp signal.

4. AUTO-ADAPTIVE PRF TECHNIQUE

According to discipline of traditional PFA, data can only be processed when they are uniformly spaced in azimuth direction. To satisfy this premise, azimuth data should be uniformly sampled. Then $\tan(\Delta\alpha)$ should be uniformly spaced as

$$\Delta\alpha(n) = \tan^{-1}\left(n\frac{\tan(\Delta\alpha_{\max}/2)}{N_a/2}\right),\quad n = -\frac{N_a}{2},\ldots,-\frac{N_a}{2} \quad (18)$$

where $\Delta\alpha_{\max}$ denotes the entire deflection of α; n is azimuth sampling serial number.

Substituting (18) into (11), $x(n)$ in ellipse trajectory mode can be expressed as

$$x(n) = R\frac{\frac{\tan(\Delta\alpha_{\max}/2)}{N_a/2}n + \sin\alpha_0}{\cos\alpha_0 - \sin\alpha_0\frac{\tan(\Delta\alpha_{\max}/2)}{N_a/2}n}\cos\psi,\ n = -\frac{N_a}{2},\ldots,-\frac{N_a}{2} \quad (19)$$

Substituting (18) into (16), $x(n)$ in hyperbola trajectory mode can be expressed as

$$x(n) = H\sin\left(\tan^{-1}\left(n\frac{\tan(\Delta\alpha_{\max}/2)}{N_a/2}\right)\right)\cot\left(\arccos\left(\frac{\cos\psi}{\cos\left(\tan^{-1}\left(n\frac{\tan(\Delta\alpha_{\max}/2)}{N_a/2}\right) + \alpha_0\right)}\right)\right),$$
$$n = -\frac{N_a}{2},\ldots,-\frac{N_a}{2} \quad (20)$$

Arc length of ellipse, circle or hyperbola between two arbitrary adjacent sample points can be computed using:

$$L(n) = \int_{x(n)}^{x(n+1)}\sqrt{1 + f'(x(n))^2}dx(n) \quad (21)$$

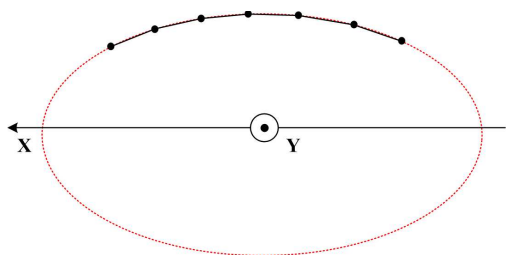

Figure 6. Lineal approximation method.

However, integration will induce heavy computation load and decrease processing speed. To simplify sensor controlling, lineal distance between two adjacent azimuth points can be approximated as arc length. Figure 6 illustrates this approximate method using ellipse trajectory mode with inspecting direction from positive Y axis. Simulation presented in Section 5 proves the validity of this approximation method.

Given that the flight velocity remains unchanged in the entire data sampling processing, PRF changing discipline for all the four space geometries is achieved by

$$\mathrm{PRF}(n) = \frac{1}{T(n)} = \frac{V}{L(n)} \tag{22}$$

where V is velocity of sensor.

By adopting this auto-adaptive PRF method, the entire computation load only includes range FFTs and azimuth CZTs after RVP compensation.

After range FFTs and azimuth CZTs processing, we get the final expression of imaged scene as Equation (23).

$$\begin{aligned} S'_{if}(k,n) \;=\; & A\exp\left\{-j\frac{4\pi}{c}f_c y\right\}\frac{\sin\left\{\pi\left(\frac{2B}{c}\left(\frac{2N_r+1}{2N_r}\right)y-k\right)\right\}}{\sin\left\{\frac{\pi}{2N_r+1}\left(\frac{2B}{c}\left(\frac{2N_r+1}{2N_r}\right)y-k\right)\right\}} \\ & \cdot\frac{\sin\left\{\pi\left(\frac{4\tan(\Delta\alpha_{\max}/2)f_c}{c}\left(\frac{2N_a+1}{2N_a}\right)x-n\right)\right\}}{\sin\left\{\frac{\pi}{2N_a+1}\left(\frac{4\tan(\Delta\alpha_{\max}/2)f_c}{c}\left(\frac{2N_a+1}{2N_a}\right)x-n\right)\right\}} \\ & k=-\frac{N_r}{2},\ldots,-\frac{N_r}{2};\quad n=-\frac{N_a}{2},\ldots,-\frac{N_a}{2} \end{aligned} \tag{23}$$

Based on analysis stated above, PFA algorithm processing shown in Figure 3 can be simplified as shown in Figure 7.

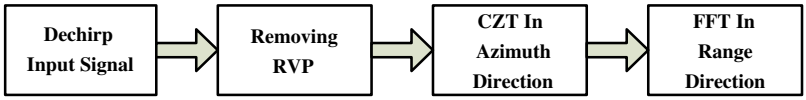

Figure 7. Flowchart of PFA using non-lineal flight trajectory and auto-adaptive PRF method.

Table 1. Targets locations in simulation.

(300, 0, 0)	(−300, 0, 0)	(0, 300, 0)
(0, −300, 0)	(0, 0, 0)	(212, 212, 0)
(212, −212, 0)	(−212, 212, 0)	(−212, −212, 0)

Table 2. Parameters for the simulation.

Parameter	**Value**
Wavelength	1.875 cm
Pulse duration	3 μs
Integration angle	5.37°
Bandwidth	1.5 GHz
Sensor velocity	100 m/s
Sampling frequency	1.2 GHz
Squint angle	26.565°
Scene center range	10 km
Scene radius	300 m
PRF changing rate A	1350.7 Hz–1357.6 Hz
PRF changing rate B	1325.2 Hz–1357.6 Hz
*Altitude	6 km

***Altitude is the parameter for fixed altitude hyperbola trajectory, PRF changing rate A and B depicts ellipse trajectory mode and hyperbola trajectory mode respectively.**

5. SIMULATION AND ANALYSIS

In this section, the presented algorithm is validated by the point target simulation. Nine simulated point targets are arranged to form a circle in ground plane (Table 1 depicts their locations). A Ku-Band LFM transmission signal is adopted for simulation. Assume that the theoretical resolution both in range and azimuth dimension

are 0.1 m. Parameters listed in Table 2 are used for computer simulation. We focus on geometry displayed in Figure 4 to make ellipse trajectory mode simulation in Section 5.1. Comparatively, we choose the geometry shown in Figure 5 to make hyperbola trajectory simulation in Section 5.2. Then simulation results and some detailed analysis are represented in Section 5.3.

5.1. Ellipse Trajectory Mode Simulation

Data are collected in geometry depicted by Figure 4. Related simulation parameters are listed in Table 2, and the resulted PFA image is shown in Figure 8(a). As for generality, we choose 2-D impulse response function (IRF) of point A to check precision of algorithm. Contour plot of IRF is given in Figure 8(b). Range and azimuth profiles are displayed in Figures 8(c) and 8(d), respectively. Peak sidelobe ratio (PSLR) and integral sidelobe ratio (ISLR) analyzing results are listed in Table 3. Eight reflectors are placed on a circle of radius 300 m, and one is set at the scene centre as shown in Table 1.

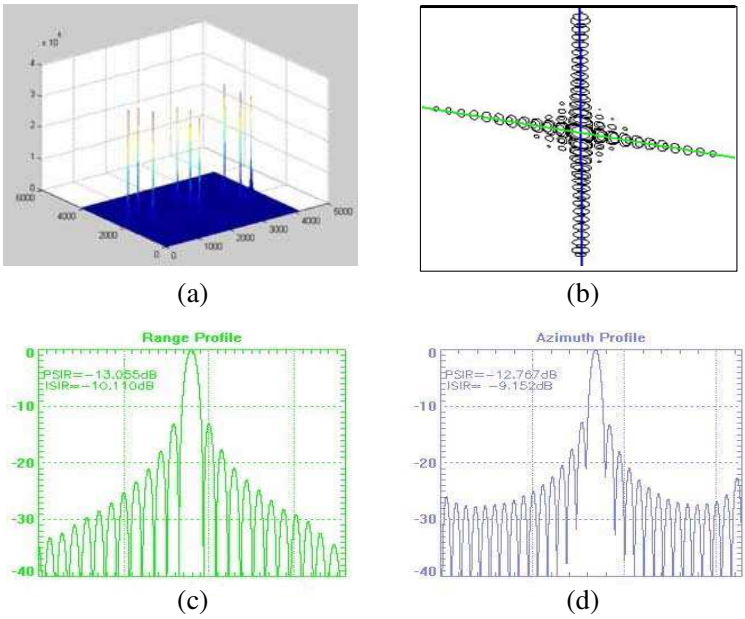

Figure 8. Imaging results and image quality inspection for ellipse trajectory mode.

Table 3. Image quality inspection for point A.

	Range		Azimuth	
	PSLR (dB)	ISLR (dB)	PSLR (dB)	ISLR (dB)
Measured value	−13.06	−10.11	−12.77	−9.15
Theoretical value	−13.26	−9.80	−13.26	−9.80

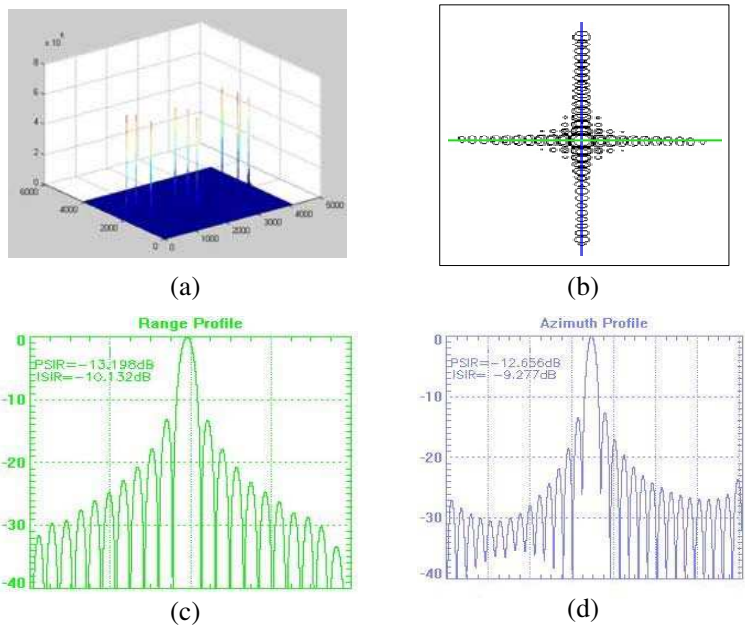

Figure 9. Imaging results and image quality inspection for hyperbola trajectory mode.

5.2. Hyperbola Trajectory Mode simulation

When sensor moves with a constant altitude, the flight path is part of a hyperbola arc. Projection of LOS on XOY plane is overlapped with the symmetry axis of hyperbola path. For comparative analysis, we still adopt parameters listed in Table 2. Figure 9(a) shows the imaging result. Figure 9(b) gives IRF of Point B without losing generality. Figures 9(c) and 9(d) present range and azimuth profiles. Detailed PSLR and ISLR inspections are listed in Table 4. Eight reflectors are placed on a circle of radius 300 m, and one is set at the scene centre as shown in Table 1.

Table 4. Image quality inspection for point B.

	Range		Azimuth	
	PSLR (dB)	ISLR (dB)	PSLR (dB)	ISLR (dB)
Measured value	−13.20	−10.13	−12.66	−9.28
Theoretical value	−13.26	−9.80	−13.26	−9.80

5.3. Analysis

As data shown in Tables 3 and 4, the measured PSLR and ISLR values correspond well with the theoretical ones, which validates this novel PFA algorithm. Inspecting range and azimuth profiles, trivial asymmetry sidelobe exists in both ellipse trajectory mode and hyperbola trajectory mode, which is caused by plane wavefront assumption and lineal approximation between two adjacent azimuth positions. However, the asymmetry property occurs at nearly −25 dB in Figure 8(d) and −30 dB in Figure 9(d). Their effects on the final imaging quality are so trivial that ISLR and PSLR standard remains very close to the theoretical level. By adopting the lineal approximation method, computational load for controlling system is further released.

By observing derivation of this trajectory-based algorithm, we find no squint angle limit is specially required, which means that SAR can image interested regions with high squint angle using this trajectory-based PFA. However, as azimuth resolution is determined by cone angle interval as discussed in [7], and accumulating time will be increased in large squint angle mode. This may put forward new challenges for stability of sensor flight.

Comparison of computation load of this new PFA and traditional PFA is presented in Appendix B. Considering azimuth process, either CZT or interpolation methods are analyzed for this trajectory-based PFA. Compared with traditional PFA, the new PFA can contribute to both a higher precision using CZT technique [15] and a faster calculation speed using interpolation process. Compared with traditional PFA, under the same resolution condition, this trajectory-based PFA requires longer accumulating time because for a certain cone angle interval and the same speed, the length of curved trajectory is longer than that in strait route. However, with its improvement in image quality and calculation speed, such time extension is worthwhile.

To ensure that images are ideally focused, phase error caused by plane wavefront assumption should be less than $\pi/4$. By applying

scene limit analyzing method introduced in [14], the scene limit ($-D_x$, $-D_y$) should be restricted by

$$D_x \leq 2\rho_a \sqrt{\frac{R_{ref}}{\lambda}} \quad D_y \leq \rho_a \sqrt{\frac{2R_{ref}}{\lambda}} \tag{24}$$

We can conclude from Equation (24) that a further illuminating distance and higher carrier frequency will contribute to a larger image region. Substituting parameters listed in Table 2, the max scene width in simulation should be (−460.1 m, 460.1 m) in azimuth direction and (−326.6 m, 326.6 m) in range direction. A 300 m scene radius as used in simulation can be ideally focused, which accords well with this scene limit analysis.

As high resolution SAR system has potential importance both in military inspection and commercial occasions, this paper chooses a Ku-Band signal to get a 0.1 m resolution both in range and azimuth direction. [16] introduces a UAV SAR experiment with 0.1 m resolution in spotlight mode. As reported, some helicopters, such as AS 350 B3 helicopter, can reach an altitude more than 8000 m. RQ-4 Global Hawk, the UAV equipped in US army, has an service ceiling of 19812 m. Moreover, the unmanned autonomous helicopter, such as MQ-8, can also have a 6100 m service ceiling. The aerial vehicles mentioned above can all be controlled in a relative low speed to implement special flight trajectory controlling as required in this trajectory-based PFA.

6. CONCLUSION

In this paper, a novel PFA using non-lineal flight trajectory and auto-adaptive PRF technique is presented. Based on geometry analysis, if sensor moves in conical surface with symmetry axis overlapping with the projection of LOS direction on XOY ground plane, interpolation can be avoided. To uniformly sample data along azimuth position, an auto-adaptive PRF technique is employed. Then azimuth CZTs finish the imaging process. The entire computation load is just left to azimuth CZTs and range FFTs.

In detailed analysis, two typical flight modes are chosen: ellipse trajectory mode and hyperbola trajectory mode. Points target simulation validates this new PFA algorithm. Considering heavy computation load of curve length integration, a lineal approximation method is proposed. Simulation demonstrates that the error caused by such an approximation can be neglected.

As squint angle is not special limited, this algorithm is suitable for highly squinted data processing. Given that numberless curves can be drawn in surface of cone, flight path can be designed flexibly

depending on real cases. Although this algorithm acquires more precision for navigation and guidance system, improvement in SAR imaging processing speed is worthwhile. Moreover, by reducing medium processing steps, accumulated error could be less than that of traditional PFA algorithm.

Compared with traditional PFA, this trajectory-based PFA has advantages of saving computation load, improving image quality and enabling large squint angle mode. It has potential value in either military or commercial usages. Further work includes new trajectories designs, real time processing [17], and bistatic SAR applications [18].

To realize fast trajectory computation, angle values which sensor needs to adjust in each azimuth sample positions can be previously computed and stored in table based on geometry and velocity information. Then based on the very angle table, computation time in trajectory control can be largely decreased. This is a tentative method to greatly save position calculation time. Future work may also focus in this direction.

ACKNOWLEDGMENT

The authors would like to thank the anonymous reviewers for their valuable comments and useful suggestions.

APPENDIX A. DERIVATION OF FLIGHT PATH SHAPE IN SQUINT MODE IN ELLIPSE TRAJECTORY MODE

As shown in Figure 4, the cone with $X'OY'$ Coordinate can be expressed as

$$y'^2 \tan^2 \psi = z^2 + x'^2 \tag{A1}$$

When radar works in squint mode, we can equal this question as to rotate the coordinate from $X'Y'Z'$ to XYZ. Sensor moves within plane $y = y_0$, for the following analysis, expression of cone in the new XYZ coordinate need to be known

We achieve coordinate relationship between $X'Y'Z'$ and XYZ

$$\begin{cases} x' = x\cos\alpha_0 - y\sin\alpha_0 \\ y' = x\sin\alpha_0 + y\cos\alpha_0 \end{cases} \tag{A2}$$

Then substituting (A2) into (A1)

$$(x\sin\alpha_0 + y\cos\alpha_0)^2 \tan^2\psi = z^2 + (x\cos\alpha_0 - y\sin\alpha_0)^2 \tag{A3}$$

Simplify (A3), we have

$$\frac{z^2}{C+\frac{B^2}{A}}+\frac{\left(x-\frac{By_0}{A}\right)^2}{\frac{C}{A}+\frac{B^2}{A^2}}=1 \tag{A4}$$

where

$$\begin{aligned} A &= \cos^2\alpha_0-\sin^2\alpha_0\tan^2\psi \\ B &= y_0\sin\alpha_0\cos\alpha_0\left(\tan^2\psi+1\right) \\ C &= y_0^2\left(\cos^2\alpha_0\tan^2\psi-\sin^2\alpha_0\right) \end{aligned} \tag{A5}$$

By observing the expression of intersection line, it can be concluded that trajectory of sensor should have an ellipse shape.

APPENDIX B. COMPARISON OF COMPUTATION LOAD OF TRADITIONAL PFA AND THIS TRAJECTORY-BASED PFA

Amount of complex multiplications is adopted as computation load indicator. To compute a single data, just assuming 16-point interpolation is adopted, 16 complex multiplications are required. Assume the sampled data has a $N_a \times N_r$ size. N_a represents the azimuth sample number. N_r represents the range sample number.

In traditional PFA, both range interpolation and azimuth interpolation requires $16N_aN_r$ complex multiplications. Then two cascade 1-D FFTs will finish the imaging reconstruction performance by leading to $(N_aN_r\log_2 N_r + N_rN_a\log_2 N_a)$ complex multiplications. C_1 represent the entire number of complex multiplications for conditional PFA.

$$C_1 = N_aN_r\log_2 N_r + N_rN_a\log_2 N_a + 32N_aN_r \tag{B1}$$

For this trajectory-based PFA, the computation amount includes Azimuth CZTs and Range FFTs. To complete CZTs $3N_aN_r\log_2 N_a + 11N_aN_r$ multiplications are needed. Range FFTs require $N_aN_r\log_2 N_r$ complex multiplications. The entire computation load C_2 is

$$C_2 = 3N_aN_r\log_2 N_a + N_aN_r\log_2 N_r + 11N_aN_r \tag{B2}$$

Assume that ρ is defined as

$$\rho = \frac{C_2}{C_1} \tag{B3}$$

Considering $N_r = 4096$, $N_a = 16384$ in simulation in Section 5, $\rho = 1.12$. As discussed in [15], CZT can contribute to a higher image precision than traditional interpolation method. However,

compared with traditional interpolation and FFT, CZT may lead to more computation load. This is the reason why ρ is larger than 1. If point-by-point interpolation can satisfy the image quality requirement, CZT may be replaced by azimuth interpolation in azimuth process. In this way, the entire computation load of new PFA is

$$C_3 = N_a N_r \log_2 N_r + 16 N_a N_r \tag{B4}$$

Using parameters adopted in Section 5, $\rho = 0.48$. This means, under the same accuracy condition, trajectory-based PFA can save a half of the entire computation load.

REFERENCES

1. Seo, D.-K., K.-T. Kim, I.-S. Choi, and H.-T. Kim, "Wide-angle radar target recognition with subclass concept," *Progress In Electromagnetics Research*, Vol. 44, 231–248, 2004.
2. Kong, J. A., S. H. Yueh, H. H. Lim, R. T. Shin, and J. J. van Zyl, "Classification of earth terrain using polarimetric synthetic aperture radar images," *Progress In Electromagnetics Research*, Vol. 3, 327–370, 1990.
3. Luo, W., M. Zhang, Y. W. Zhao, and H. Chen, "An efficient hybrid high-frequency solution for the composite scattering of the ship on very large two-dimensional sea surface," *Progress In Electromagnetics Research M*, Vol. 8, 79–89, 2009.
4. Tian, B., D.-Y. Zhu, and Z.-D. Zhu, "A novel moving target detection approach for dual-channel SAR system," *Progress In Electromagnetics Research*, Vol. 115, 191–206, 2011.
5. Mao, X., D.-Y. Zhu, L. Ding, and Z.-D. Zhu, "Comparative study of RMA and PFA on their responses to moving target," *Progress In Electromagnetics Research*, Vol. 110, 103–124, 2010.
6. Mao, X. H., D.-Y. Zhu, and Z.-D. Zhu, "Signatures of moving target in polar format spotlight SAR image," *Progress In Electromagnetics Research*, Vol. 92, 47–64, 2009.
7. Carrara, W. G., R. S. Goodman, and R. M. Majewski, *Spotlight Synthetic Aperture Radar*, Artech House, MA, USA, 1995.
8. Moreira, A., J. Mitterayer, and R. Scheiber, "Extended chirp scaling algorithm for air and spaceborne SAR data processing in stripmap and scan SAR imaging modes," *IEEE Trans. Geosci. Remote Sens.*, Vol. 34, No. 5, 1123–1136, 1996.
9. Guo, D., H. Xu, and J. Li, "Extended wavenumber domain algorithm for highly squinted sliding spotlight SAR data

processing," *Progress In Electromagnetics Research*, Vol. 114, 17–32, 2011.

10. Jakowatz, C. V., D. E. Wahl, D. D. Ghiglia, and P. A. Thompson, *Spotlight-mode Synthetic Aperture Radar: A Signal Processing Approach*, Kluwer Academic Publishers, 1996.
11. Mittermayer, J., A. Moreira, and O. Loffeld, "Spotlight SAR data processing using the frequency scaling algorithm," *IEEE Trans. Geosci. Remote Sens.*, Vol. 37, No. 5, 2198–2214, 1999.
12. Desai, M. and W. Jenkins, "Convolution back projection image reconstruction for spotlight mode synthetic aperture radar," *IEEE Trans. Image Process.*, Vol. 1, No. 4, 505–517, 1992.
13. Yuan, Y., J. Sun, and S. Mao, "PFA algorithm for airborne spotlight SAR imaging with non-ideal motions," *IEE Proc. Radar Sonar Navig.*, Vol. 149, No. 4, Aug. 2002.
14. Bao, Z., M. D. Xing, and T. Wang, *Radar Imaging Technique*, Publishing House of Electronics Industry, Beijing, China, 2008.
15. Tang, Y., M. D. Xing, and Z. Bao, "The polar format imaging algorithm based on double chirp-Z transforms," *IEEE Geoscience and Remote Sensing Letters*, Vol. 5, No. 4, Oct. 2008.
16. Tsunoda, S. I., F. Pace, J. Stence, M. Woodring, W. H. Hensley, A. W. Doerry, and B. C. Walker, "Lynx: A high-resolution synthetic aperture radar," *SPIE Aerosense*, Vol. 3704, 1999.
17. Chan, Y. K., V. C. Koo, B.-K. Chung, and H.-T. Chuah, "Modified algorithm for real time SAR signal processing," *Progress In Electromagnetics Research C*, Vol. 1, 159–168, 2008.
18. Sun, J., S. Mao, G. Wang, and W. Hong, "Polar format algorithm for spotlight bistatic SAR with arbitrary geometry configuration," *Progress In Electromagnetics Research*, Vol. 103, 323–338, 2010.